Journal of Thermal Analysis, Vol. 42 (1994) 159-174

Dedicated to Professor Lisa Heller-Kallai on the occasion of her 65th birthday

THERMOGRAVIMETRIC EVALUATION OF THE KINETICS OF THE GYPSUM–HEMIHYDRATE–SOLUBLE ANHYDRITE TRANSITIONS

Y. Deutsch[1], *Y. Nathan*[1] *and S. Sarig*[2]

[1] Geological Survey of Israel, 30 Malchei Israel St. Jerusalem 95501, Israel
[2] Casali Institute, Hebrew University of Jerusalem, Israel

Abstract

Study of the gypsum–hemihydrate–soluble anhydrite transitions by thermal, X-ray and IR methods showed differences in the intensity of the ~3493 cm^{-1} IR absorption peak of the gypsum samples and differences in the peak ratios of the DTA curve at the gypsum–hemihydrate transition. There were also differences in the temperature and rate of the $\gamma - \beta$ anhydrite transition. This suggests that different gypsum species occur, specially among synthetic gypsum.

Fifteen equations were tested in order to find models which fitted the gypsum–hemihydrate and the hemihydrate–anhydrite transitions. No model fitted all the samples. The best fit for the gypsum–hemihydrate transition in three samples was an order of reaction equation while for the hemihydrate–anhydrite transition the best fit in four samples was a power law. Differences in crystallite characteristics appear to be one of the main reasons for the differences in kinetics between the samples.

Keywords: gypsum–hemihydrate–soluble anhydrite transitions, kinetics, TG

Introduction

The temperature of dehydration of gypsum ($CaSO_4 \cdot 2H_2O$) was already investigated in 1887 by Le Chatelier (quoted by Groves, [1]). He observed a two-step dehydration: a loss of 1.5 water molecules at 128°C leading to the formation of hemihydrate followed by the loss of a further 0.5 molecule of water at 163°C producing soluble anhydrite. Many authors have dealt with various aspects of the dehydration, among others, van't Hoff *et al.*, [2] who stressed the influence of pressure. The latter showed that at 970 mm (Hg) pressure, gypsum dehydrates into hemihydrate at 107°C; at 588, 254 and 105 mm (Hg) pressure, gypsum dehydrates to soluble anhydrite at 93, 72 and 60°C respectively; and at a pressure of 175 mm, gypsum transforms to insoluble anhydrite already at

0368–4466/94/ $ 4.00

John Wiley & Sons, Limited
Chichester

63.5°C. Bish and Duffy, [3] showed the influence of particle size, i.e., the dehydration temperatures decreases with decrease in particle size. Paulik *et al.* [4] showed the influence of several experimental parameters such as: type of sample holder, heating rate and amount of sample. From thermodynamic considerations, Hardie [5] found 58°C to be the temperature for the gypsum–hemihydrate transition at one atmosphere pressure, Wiedeman and Rossler [6] found 40°C while Hamad [7] found it to be 46°C.

Numerous phases occur in the $CaSO_4 - H_2O$ system, of which the following are dealt with, in this study: a) the dihydrate, $CaSO_4 \cdot 2H_2O$, termed gypsum; b) the two varieties of hemihydrate, $CaSO_4 \cdot 0.5H_2O$: β-hemihydrate, the more common variety, obtained when gypsum is heated at atmospheric pressure, and α-hemihydrate which is obtained by heating gypsum under relatively high pressures of water vapour [8] (at least 0.14 MPa); c) two of the anhydrite, $CaSO_4$, species, are considered: γ-anhydrite, the so-called soluble anhydrite, is obtained by heating β-hemihydrate; further heating transforms it into β-anhydrite (the more common natural variety, the so-called insoluble anhydrite). α-hemihydrate is transformed directly (without going through γ-anhydrite) into β-anhydrite on heating.

The wide range of temperatures quoted in the literature for the above mentioned transitions at atmospheric pressure, is probably the result of kinetics. The aim of the present work is to investigate the kinetics of these reactions by thermogravimetry. Isothermal experiments were preferred to the normal dynamic thermogravimetric runs [9]. The kinetics of gypsum dehydration were already studied inter alia by Khalil (using only one gypsum sample) [10].

The dehydration process

The dehydration of gypsum (and hemihydrate) in the thermobalance comprises at least three steps [3]: 1) breaking the bonds involving the water molecules; 2) diffusion of the water molecules through the crystals, the initial phase and the newly formed phase; 3) transport of the water molecules from the pore spaces to the purge gas. The sample geometry and different conditions cause variations in the relative importance of these processes. The gypsum–hemihydrate transition involves, apart from the expulsion of water, a reordering of the Ca^{2+} and SO_4^{2-} ions. The lattice changes from monoclinic to orthorombic, shrinks by about 29%, from a volume of 124 $Å^3$ for the gypsum unit cell to the 88 $Å^3$ hemihydrate unit cell and the density increases from 2.31 $g \cdot cm^{-3}$ to 2.73 $g \cdot cm^{-3}$. The remaining water molecules in hemihydrate are positioned in the hexagonal canals built by the tetrahedral SO_4^{2-} anions and the Ca^{2+} cations [11]. This explains why the transition from hemihydrate to soluble anhydrite (γ-

$CaSO_4$) causes practically no changes in the structure as can be seen from the X-ray pattern (Fig. 1). The expulsion of the remaining 0.5 water molecules without structural changes reduces the density (D_x) from 2.73 to 2.53 g·cm^{-1}. There is almost no volume difference between the unit cells (per formula) of soluble anhydrite (89.2 Å^3) and hemihydrate (88.3 Å^3). The difference in density is due solely to the removal of water.

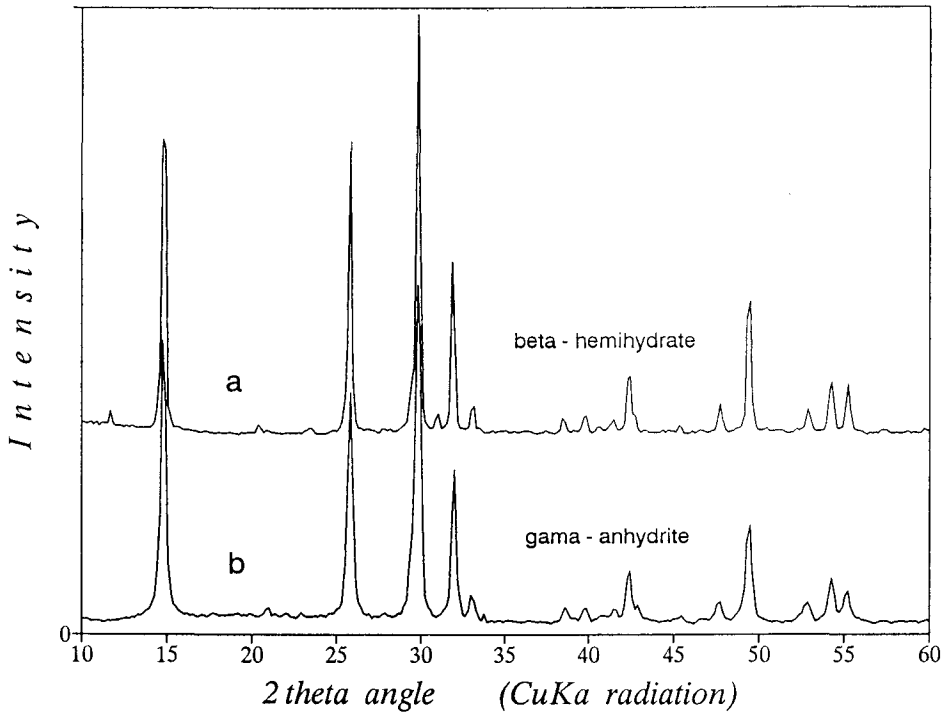

Fig. 1 XRD diffractograms, a) β-hemihydrate; b) γ-anhydrite. The diffractograms cannot be differentiated apart from two small gypsum peaks which occur in the β-hemihydrate diffractogram

Experimental

Samples

Five gypsum samples were used in this study: a) two natural samples: a selenite sample from the Gesher quarry (Jordan valley) and a satin spar sample from the Ramon quarry (Negev); b) three synthetic samples (pure chemicals) obtained from British Drug House Ltd. (Analar® , BDH), E. Merck Ltd. (Pro analysi® , Merck) and Johnson Matthey Ltd. (Specpure® , JMC).

Infrared (IR)

Alkali halide discs were prepared by mixing 1 mg of the ground sample with 150 mg KBr. The mixtures were ground in an agate mortar and mixed manually before the disc was pressed. The infrared absorption spectra were recorded on a Nicolet ZDX FT-IR spectrometer.

X-ray diffraction (XRD)

All the XRD's were carried out with a Philips diffractometer (PW-1820/00 with a monochromator PW-1752/00), with 1° divergence slit, 0.2 mm receiving slit and 1° scatter slit using a long fine focus Cu tube. XRD was used: a) to identify the various phases; for this purpose the step size was 0.02° 2Θ and the scanning speed 1.5° 2Θ/min. Samples taken after the thermal runs were run immediately to avoid rehydration; b) to obtain an order of magnitude for the crystallite size from the Scherrer equation ([12], p. 687–704). In this case a smaller scanning speed was chosen with step size of 0.02° 2Θ and scanning speed 0.6° 2Θ/min.

The JCPDS ICDD now have two cards for gypsum: 21–816 obtained from a transmission-type camera from a non-oriented, "normal" sample and 33-311 acquired from a diffractometer (sample with a preferred orientation). The differences between the two patterns are mainly in the relative intensities. Grattan-Bellew [13] showed the relationships between preferred orientation an intensities in gypsum. Only one card, 33–310, now accounts for hemihydrate (termed synthetic bassanite). There are two more cards for $CaSO_4$ with different water contents, 23–128, with 0.15 H_2O and 36–617, with 0.67 H_2O. There are two cards for γ-anhydrite (soluble anhydrite) 26–329 and 37–184. However, the data in 37–184 is very different from that in 26–329 and is almost identical that in 37–1496 which is the card for β-anhydrite (insoluble anhydrite). It is therefore recommended to delete 37–184 from the card index.

Thermal analysis (DTA and TG)

The thermal analysis were carried out with a Stanton-Redcroft (STA 781) instrument. This is an apparatus which runs differential thermal analysis (DTA) and thermogravimetric analysis (TG) simultaneously. Platinum sample holders, with a diameter of 5.5 mm and a height of 4 mm, were used. 20.5± 0.5 mg of pure sample and of α-alumina (reference) were used. Dynamic simultaneous DTA-TG runs were carried out (10 deg·min^{-1}) with dry air as purge gas in the range of ambient up to 1250°C. Isothermal runs at 40, 50, 60, 70 and 90°C were kept at the required temperature until the reaction ended or no change whatso-

ever was found after a week. All the samples were run with a purge gas, most with dry air and some with "humid" air.

Results

IR

The absorption curves are given in Fig. 2. The spectra were obtained in the 400–4000 cm^{-1} range. Gypsum has four vibration bands (H–O–H stretching) in the 3200–3600 cm^{-1} region [14, 15]. Only very small differences could be observed up to 3400 cm^{-1} between the various gypsum spectra. However, significant differences were observed in two vibration bands at about 3500 and 3555 cm^{-1} in the H–O–H stretching region. The data for the four bands, (marked 1–4 in Fig. 2) in the 5 samples studied is given in Table 1. The precision of the band position is ± 2 cm^{-1}.

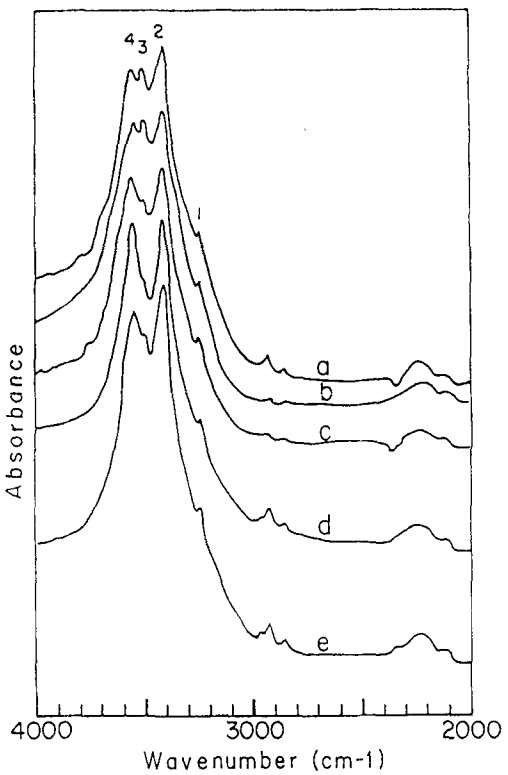

Fig. 2 IR absorption curves, a) JMC; b) BDH; c) Merck; d) satin spar; e) selenite, showing the four vibration bands in the H–O–H stretching region

Table 1 Position and assignment of IR spectra in the 3200–3600 cm^{-1} region

JMC	BDH	Merck	Satin spar	Selenite	Assignment
3243vw	3243vw	3244vw	3244vw	3245vw	$2 \times \nu_2H_2O$, ν_3H_2O
3405vs	3405vs	3405vs	3405vs	3405vs	ν_1H_2O
3493m	3493m	3493w	3498sh	3503vw	ν_1H_2O
3546s	3548s	3551s	3550vs	3547m	ν_3H_2O

sh – shoulder, vw – very weak, w – weak, m – medium, s – strong, vs – very strong

XRD

No differences were observed in the position of the peaks in the diffractograms of the 5 gypsum samples. On the other hand, some differences could be observed in the crystallites size as determined from line broadening. These are reflected in the dimensions of $L_{(020)}$, in angstroms, of the five samples and are shown in Table 2. $L_{(hkl)}$ is the mean dimension of the crystallites composing the powder in the (hkl) direction, and was evaluated from the Scherrer equation, $L = K\lambda/\beta \cos\Theta$ [12]. Although the accuracy in measuring the instrumental broadening is rather low, making the absolute value of crystallite size uncertain, the accuracy of the relative sizes is fair.

Table 2 Size of $L_{(020)}$ of the gypsum samples

Sample	JMC	BDH	Merck	Satin spar	Selenite
$L_{(020)}$ /Å	2200	2600	2900	3100	3000

Thermal analysis

Figure 3 shows the traces of the dynamic DTA of the three synthetic samples together with a generalized TG curve. It can be seen that the three DTA traces are different from each other. All of the gypsum samples run in our laboratory (the five samples dealt with in the present work and tens of others) were similar to one of the three patterns shown in Fig. 3. Most samples had a DTA trace similar to the BDH gypsum (a). In this pattern the five two endothermic peaks have a 3:1 ratio (equal to the water loss, 1.5:0.5). The soluble-insoluble anhydrite transition is represented by an exothermic peak at about 380°C. In the Merck sample, the ratio of the first two peaks is almost (slightly less than) unity. The exothermic peak, soluble – shows the best resolution for the first two endothermic peaks, for the experimental conditions used, and their ratio is 5:1 or even more. The exothermic peak is much less pronounced and occurs at lower temperatures adjacent to the endothermic peaks. Differences were also observed in the patterns, in the high temperature range, of the β-anhydrite – α-anhydrite transition(s).

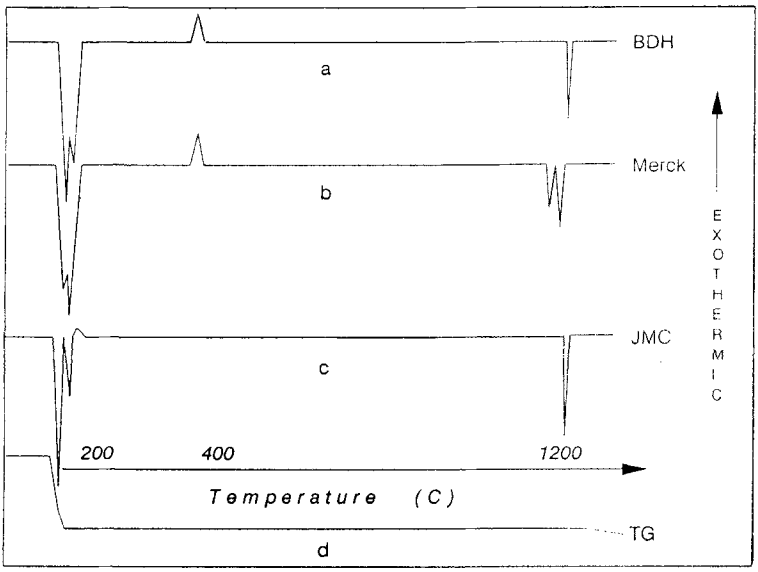

Fig. 3 DTA traces of synthetic gypsum samples (chemicals), a) BDH; b) Merck; c) JMC, and d) a generalized TG curve

Table 3 Times needed for the gypsum-hemihydrate transition (isothermal conditions)

Temperature/°C	JMC	BDH	Merck	Satin spar	Selenite
40	72 h	No loss	No loss	No loss	No loss
50	34 h	No loss	very slow loss	No loss	No loss
60	minutes	50 h	90 h	65 h	85 h
70	minutes	16 h	16 h	20 h	44 h
90	seconds	3 h	3 h	4 h	5 h

No loss – No weight loss after one week

The results of the isothermal thermogravimetric analyses (dry air) are summarized in Tables 3 and 4, and Figs 4a and 4b show them for 60 and 90°C. Table 3 gives the approximate times needed for the transition gypsum–hemihydrate at the various temperatures and Table 4, the times needed for the gypsum – sol-

Table 4 Times needed for the hemihydrate – anhydrite transition (isothermal conditions)

Temperature/°C	JMC	BDH	Merck	Satin spar	Selenite
40	No loss	No loss	No loss	No loss	No loss
50	very slow loss	No loss	No loss	No loss	No loss
60	30 h	90 h	160 h	100 h	130 h
70	5 h	24 h	22 h	50 h	72 h
90	<1 h	5 h	5 h	6 h	8 h

uble anhydrite transition. As a rule, the dehydration occurs at lower temperatures in the synthetic samples. The reason for the relatively low temperatures we obtained is due to the isothermal conditions we used. In the usual conditions (dynamic thermogravimetric runs) temperatures between 100 to 130°C are obtained for the gypsum–hemihydrate transition.

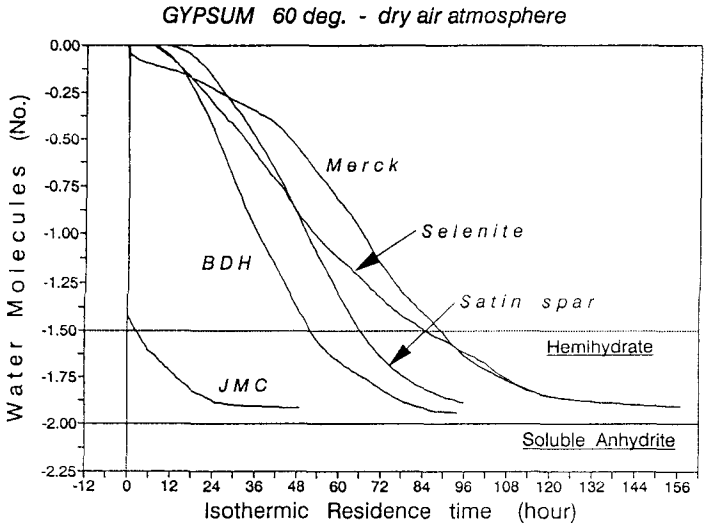

Fig. 4 a) Isothermal gypsum–hemihydrate and anhydrite transitions at 60°C

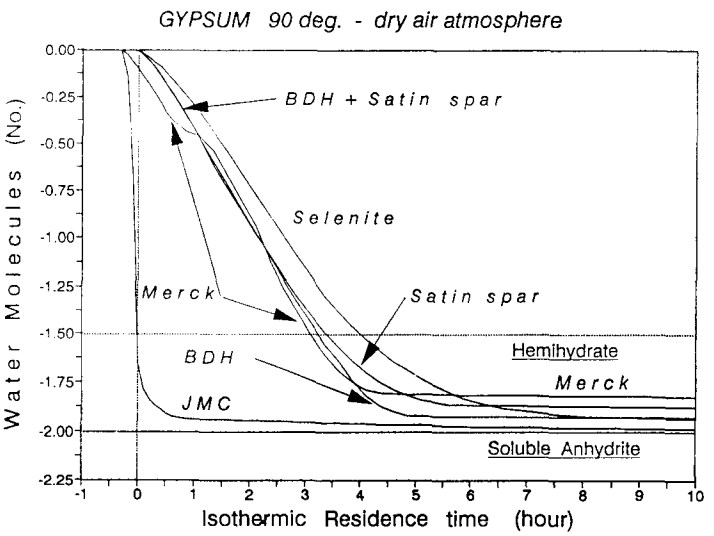

Fig. 4 b) Isothermal gypsum – hemihydrate and anhydrite transitions at 90°C

Kinetic models and discussion

The thermal dehydration of gypsum can be represented by the following two solid state reactions (e.g., Paulik *et al.*, 1992, [4]):

a)	Gypsum	→	Hemihydrate	+	Water vapor	
	$CaSO_4 \cdot 2H_2O$ (s)	→	$CaSO_4 \cdot 0.5H_2O$ (s)	+	$1.5H_2O$ (v)	(1)
b)	Hemihydrate	→	soluble anhydrite	+	Water vapor	
	$CaSO_4 \cdot 0.5H_2O$ (s)	→	$CaSO_4$ (s)	+	$0.5H_2O$ (v)	(2)

Most models of solid state reactions deal with reactions between two solids. These models are quite complex because the interface between two solids is not well understood. In our case there is only one reactant, which implies that the reaction may occur anywhere in the phase (not only at the interface). As a first approximation, the models developed for solutions were tried for these reactions. The following mathematic development is based on Freeman and Carroll [16]. For reactions 1 and 2 at equilibrium the equilibrium constant of the equations can be written:

$$K_1 = \frac{[CaSO_4 \cdot 0.5H_2O]\ [H_2O]^{1.5}}{[CaSO_4 \cdot 2H_2O]} \tag{3}$$

and

$$K_2 = \frac{[CaSO_4]\ [H_2O]^{0.5}}{[CaSO_4 \cdot 0.5H_2O]} \tag{4}$$

If we assume that activity equals 1 then the equations reduce to $K_1 = [H_2O]^{1.5}$ (3) and $K_2 = [H_2O]^{0.5}$ (4). The equilibrium constants are therefore a function of the water vapour concentration (or more exactly, its fugacity). Equations (3) and (4) are (approximately) correct only if the loss of water is the step which regulates the rate of the reaction. The rate of the reaction is described by the following equation:

$$-\frac{dC}{dt} = kC^n \tag{5}$$

when reordered

$$-\frac{dC}{C^n} = kdt \tag{6}$$

integrating (6) between concentrations C_o and C between times t_o and t we get:

$$-\int_{c_o}^{c} \frac{dc}{c^n} = k \int_{o}^{t} dt \tag{7}$$

when $n = 1$ (first order) we obtain:

$$-\ln \frac{C}{C_o} = k_1 t, \quad \ln[C] = -k_1 t + \ln[C_o]$$

Plotting $\ln[C]$ *vs.* time gives in this case a straight line whose slope equals $-k_1$ and which intersect the t-axis at $\ln[C_o]$. When $n = 2$ (second order) we obtain when integrating (7):

$$\frac{1}{[C]} - \frac{1}{[C_o]} = k_2 t, \quad \frac{1}{[C]} = k_2 t - \frac{1}{[C_o]}$$

In this case plotting $1/[C]$ *vs.* time gives a straight line whose slope is k_2 and intersects the t-axis at $1/[C_o]$.

α, the conversion fraction, is the variable generally used to describe solid state reactions; it is proportional to $1-[C]$. In general, the gypsum $\rightarrow$ hemihydrate transitions did not follow first order or second order reaction kinetics. Only in one case (JMC) was it possible to assign an order reaction (even this was doubtful, see below). The (reaction order) model was much more successful for the hemihydrate $\rightarrow$ anhydrite conversions. In two cases (BDH, Satin spar) the hemihydrate – anhydrite transition agreed with a first order reaction (for BDH, the contracting volume model is probably better, see below); in two others (Merck, JMC) with a second order reaction, and in the fifth case (Selenite) there was no agreement.

One of the factors which determine the rate of the hemihydrate – anhydrite transition is the slowest step of the dehydration reaction. Practically no structural changes occur in this transition. It is therefore probable that this step is the diffusion of water molecules through the crystals. Since experimental conditions were kept constant throughout the study, particle characteristics (see also Table 2) appear to be one of the main reasons for the kinetic differences observed in the five samples studied.

For a better understanding (mainly of the gypsum–hemihydrate reaction) a more general approach was used, based on known mathematical relationship between the conversion fraction (α) and the time of heat treatment. Table 5, taken from Dollimore [17], lists the equations which we used in an attempt to find models which fitted the gypsum – hemihydrate and the hemihydrate – anhydrite reactions in our samples.

Table 5 Mathematical models of reaction mechanisms, after Dollimore [17]

		$g(\alpha) = kt$
1) Acceleratory α – time curves		
P1	Power law	$\alpha^{1/n}$
E1	Exponential law	$\ln\alpha$
2) Sigmoidal α – time curves		
A2	Avrami-Erofeev	$[-\ln(1-\alpha)]^{1/2}$
A3	Avrami-Erofeev	$[-\ln(1-\alpha)]^{1/3}$
A4	Avrami-Erofeev	$[-\ln(1-\alpha)]^{1/4}$
B1	Prout-Tompkins	$\ln[\alpha/(1-\alpha)] + c$
3) Deceleratory α – time curves		
3.1) based on geometrical models		
R2	Contracting area	$1-(1-\alpha)^{1/2}$
R3	Contracting volume	$1-(1-\alpha)^{1/3}$
3.2) based on diffusion mechanisms		
D1	One dimensional	α^2
D2	Two dimensional	$(1-\alpha)\ln(1-\alpha)+\alpha$
D3	Three dimensional	$[1-(1-\alpha)^{1/3}]^2$
D4	Ginstling-Brounshtein	$(1-2\alpha/3)-(1-\alpha)^{2/3}$
3.3) based on order of reaction		
F1	First order	$-\ln(1-\alpha)$
F2	Second order	$1/(1-\alpha)$
F3	Third order	$[1/(1-\alpha)]^2$

Table 6 summarizes the results of isothermal heating at 60°C for the five studied gypsum samples. 60°C was chosen because at lower temperatures, the reactions are too slow for most samples and at higher temperatures, the reaction is instantaneous for JMC (even 60°C is too high for JMC to obtain enough measurements, see further on). Table 6 gives the four equations with the best linear regression (R^2, with its value), together with the number of points measured and the slope of the straight line. A point which should be taken into account is that in the initial and final stages of the dehydration, the kinetics are quite different than in the main range due to the induction period and the delayed time for the retained residual water. If these measurements are excluded (10% on each side), then, in some cases, models which were second best or worse become first. Table 7 summarizes these results and Fig. 5a gives the plot of the best fit for the gypsum to hemihydrate transition while Fig. 5b shows the plot for the worse fit for the hemihydrate to anhydrite conversion.

Table 6 The best four kinetics functions for the five gypsum samples, formula, slope and R-squared; gypsum to hemihydrate and hemihydrate to anhydrite reactions

Gypsum to Hemihydrate				Hemihydrate to Anhydrite			
		Slope	R-Squared			Slope	R-Squared
Merck	alpha ^ 1/3	0.0077	0.9956	Merck	1/(1 - alpha)	0.0742	0.9875
n = 133	alpha ^ 1/2	0.0093	0.9948	n = 68	[1/(1 - alpha)] ^ 2	0.5025	0.9843
	alpha ^ 1/4	0.0065	0.9925		[1 - (1 - alpha) ^ 1/3] ^ 2	0.0032	0.9660
	[-ln(1 - alpha)] ^ 1/4	0.0094	0.9730		(1 - 2/3alpha) - (1 - alpha) ^ 2/3	0.0022	0.9485
B.D.H.	[-ln(1 - alpha)] ^ 1/3	0.0288	0.9912	B.D.H.	-ln(1 - alpha)	0.0565	0.9910
n = 65	alpha	0.0237	0.9902	n = 42	1 - (1 - alpha) ^ 1/3	0.0130	0.9900
	[-ln(1 - alpha)] ^ 1/2	0.0366	0.9876		1 - (1 - alpha) ^ 1/2	0.0163	0.9841
	[-ln(1 - alpha)] ^ 1/4	0.0240	0.9766		alpha ^ 2	0.0222	0.9821
J.M.C.	1/(1 - alpha)	51.1780	0.8340	J.M.C.	1/(1 - alpha)	0.1316	0.9662
n = 13	-ln(1 - alpha)	1.5054	0.8195	n = 80	[1/(1 - alpha)] ^ 2	0.9178	0.9596
	[1 - (1 - alpha) ^ 1/3] ^ 2	0.2168	0.7850		[1 - (1 - alpha) ^ 1/3] ^ 2	0.0056	0.9502
	ln(alpha/(1 - alpha)]	1.6624	0.7577		(1 - 2/3alpha) - (1 - alpha) ^ 2/3	0.0039	0.9415
Selenite	alpha	0.0139	0.9952	Selenite	1 - (1 - alpha) ^ 1/2	0.0135	0.9893
n = 97	[-ln(1 - alpha)] ^ 1/3	0.0164	0.9860	n = 41	1 - (1 - alpha) ^ 1/3	0.0100	0.9889
	[-ln(1 - alpha)] ^ 1/2	0.0222	0.9816		-ln(1 - alpha)	0.0372	0.9846
	1 - (1 - alpha) ^ 1/2	0.0109	0.9806		alpha	0.0202	0.9832
Satin spar	alpha ^ 1/2	0.0180	0.9880	Satin spar	-ln(1 - alpha)	0.0507	0.9976
n = 64	alpha	0.0189	0.9830	n = 30	(1 - alpha)ln(1 - alpha) + alpha	0.0165	0.9952
	[-ln(1 - alpha)] ^ 1/3	0.0234	0.9825		alpha ^ 2	0.0226	0.9951
	[-ln(1 - alpha)] ^ 1/4	0.0193	0.9818		(1 - 2/3alpha) - (1 - alpha) ^ 2/3	0.0042	0.9925

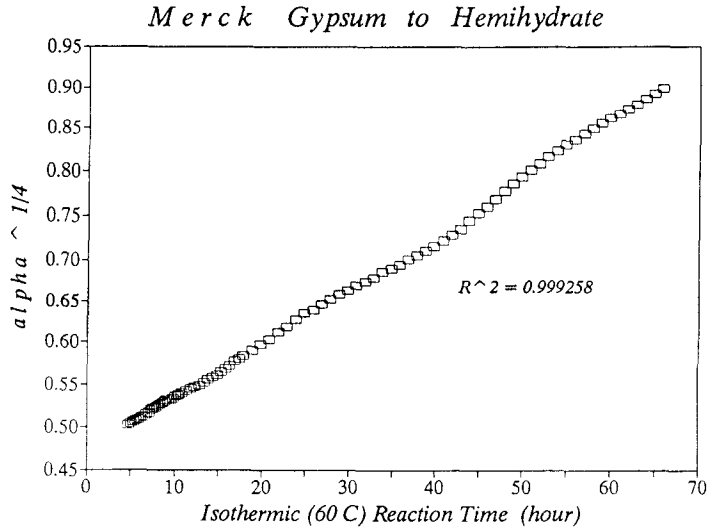

Fig. 5a Plots of $\alpha^{1/4}$ *vs.* time for the isothermal BDH gypsum to hemihydrate transition at 60°C

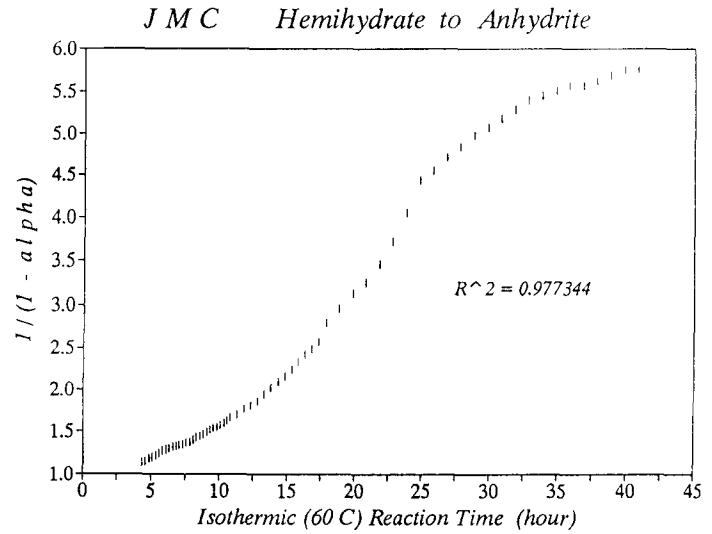

Fig. 5b Plots of $1/(1-\alpha)$ *vs.* time for the isothermal JMC hemihydrate to anhydrite transition at 60°C

It can be seen that for the gypsum – hemihydrate transition, for three samples (Merck, Selenite and Satin spar), the best model is the power law (Table 6). Without extremes, a sigmoidal α – time curve becomes the best model for Selenite and Satin spar, while for Merck the best model remains a power curve

Table 7a The two functions with the best fit (without extremes) for the gypsum to hemihydrate transition in the five gypsum samples

Sample	Equation (model)	Slope	R^2
Merck	$\alpha^{1/4}$	0.0065	0.9993
$n = 107$	$\alpha^{1/3}$	0.0077	0.9982
BDH	$[-\ln(1-\alpha)]^{1/2}$	0.0342	0.9990
$n = 53$	$[-\ln(1-\alpha)]^{1/3}$	0.0277	0.9949
JMC	$1/(1-\alpha)$	37.9789	0.9059
$n = 11$	$-\ln(1-\alpha)$	1.2491	0.8407
Selenite	$[-\ln(1-\alpha)]^{1/2}$	0.0203	0.9989
$n = 77$	$[-\ln(1-\alpha)]^{1/3}$	0.0145	0.9967
Satin spar	$[-\ln(1-\alpha)]^{1/3}$	0.0215	0.9969
$n = 52$	$\alpha^{1/2}$	0.0184	0.9913

(Table 7). For BDH, a sigmoidal α – time curve is the most appropriate in both cases. As already mentioned, a second order reaction model gives the best result for JMC (Table 6) but with an R^2 which is only 0.834. It should be remembered that there were only 13 measured points at that temperature, since at 60°C, the reaction is almost instantaneous for JMC, making the results for this temperature dubious. There was no change in the best model when extremes were excluded (Table 7).

Table 7b The two functions with the best fit (without extremes) for the hemihydrate to anhydrite transition in the five gypsum samples

Sample	Equation (model)	Slope	R^2
Merck	$[1/(1-\alpha)]^2$	0.5331	0.9911
$n = 54$	$1/(1-\alpha)$	0.0780	0.9861
BDH	$1-(1-\alpha)^{1/3}$	0.0136	0.9955
$n = 34$	$[-\ln(1-\alpha)]^{1/2}$	0.0294	0.9947
JMC	$1/(1-\alpha)$	0.1499	0.9773
$n = 64$	$[1-(1-\alpha)^{1/3}]^2$	0.0065	0.9699
Selenite	$[-\ln(1-\alpha)]^{1/2}$	0.0270	0.9932
$n = 33$	$1-(1-\alpha)^{1/2}$	0.0145	0.9928
Satin spar	$(1-\alpha)\ln(1-\alpha)+\alpha$	0.0173	0.9986
$n = 24$	$-\ln(1-\alpha)$	0.0509	0.9984

For the hemihydrate – anhydrite transition, only in one case, (Selenite), a geometrical (contracting) model was more appropriate than a model based on the order of reaction (Table 6). When extremes are excluded, the best model for Merck and JMC remains order of reaction; for BDH it changes to contracting volume, for Selenite to a sigmoidal α – time curve; and for Satin spar two-dimension diffusion.

The theory of sigmoidal α – time curves kinetic model is based on the assumption that the new phase is nucleated by germ nuclei which already exist in the old phase, their differential growth, and the ingestion of the slow-growing nuclei by fast-growing ones [18–20]. The difference between the two geometric (contracting) models is the shape of the grains involved, plate-like for the two-dimensional model and spheres for the three-dimensional.

The fact that a mathematical equation fits the experimental data does not necessarily prove a specific mechanism. Furthermore in some cases the differences between the R^2 of various equations are negligible, showing that more than one model fits the data.

Conclusions

Clear differences observed in the thermal behaviour, such as differences in peak ratios at the gypsum – hemihydrate transition, in the temperature of the γ–β anhydrite transition, and in the IR, such as differences in the intensity of the absorption peak at ~3493 cm^{-1} of the gypsum samples in this study. These suggest that different gypsum species occur, especially among synthetic gypsum.

The gypsum – hemihydrate transition appears to be quite different, from a kinetic point of view, from the hemihydrate – anhydrite transition. The best fit models for the first are acceleratory α – time curves (or sigmoidal) while for the second, deceleratory α – time curves are more appropriate. Differences in crystallite characteristics (crystallite size, amount of defects) seem to be one of the main reasons for the differences in kinetics between the samples.

* * *

We thank Dr. Shlomo Shoval for his help with the IR analysis and Prof. Itamar Pelly (Dept. of Geology, Ben-Gurion Univ.) and Dr. Henry Foner (GSI) for their critical reading of the manuscript and their constructive comments.

References

1 A.W. Groves, Gypsum and Anhydrite, Overseas Geological Surveys, London 1958, p. 108.
2 J.H. van't Hoff, E.F. Armstrong, W. Hinrichsen, F. Weigert and G. Just, Zeits. Physik. Chemie, XLV (1903) 257.

3 D.L. Bish and C.J. Duffy, CMS workshop lectures, V. 3, Thermal Analysis in Clay Science, J.W. Stucki and D.L. Bish (eds.), Clay Minerals Society (1990) 96.
4 F. Paulik, J. Paulik and M. Arnold, Thermochim. Acta, 200 (1992) 195.
5 L.A. Hardie, Am. Mineral., 52 (1967) 171.
6 H.G. Wiedeman and M. Rossler, Thermochim. Acta, 95 (1985) 145.
7 S. el D. Hamad, Sudan J. Science, 1 (1985) 48.
8 M. Gott, B. Molony, M.J. Ridge and G.W. West, Ausralian J. Chemistry, 19 (1966) 313.
9 J. Sestak, Talanta, 13 (1966) 567.
10 A.A. Khalil, Thermochim. Acta, 55 (1982) 201.
11 O.W. Florke, Neues Jb. Mineral. Abh., 84 (1952) 189.
12 H.P. Klug and L.E. Alexander, X-ray diffraction procedures, Wiley, 1974, p. 966.
13 P.E. Grattan-Bellew, Am. Mineral., 60 (1975) 1127.
14 J. Bensted and S. Prakash, Nature, 219 (1968) 60.
15 A. Putnis, B. Winkler and L. Fernandez-Diaz, Mineral. Mag., 54 (1990) 123.
16 E.S. Freeman and B. Caroll, J. Physic. Chem., 62 (1958) 394.
17 D. Dollimore, J. Thermal Anal., 38 (1992) 111.
18 M. Avrami, J. Chemical Physics, 7 (1939) 1103.
19 M. Avrami, J. Chemical Physics, 8 (1940) 212.
20 C.R. Erofeyev, In Chemistry of the Solid State, W.E. Garner (Ed.), London, Butterworths 1955, p. 184.

Zusammenfassung — Die mittels thermischen, Röntgen- und IR-Methoden untersuchte Umwandlung Gips/Halbhydrat/lösliches Anhydrat zeigte Unterschiede in der Intensität des Absorptionspeaks bei ~3493 cm^{-1} der Gipsprobe und Unterschiede bei den Peakverhältnissen der DTA-Kurve bei der Gips/Halbhydratumwandlung. Es gab auch Unterschiede bei der Temperatur und der Geschwindigkeit der γ–β-Anhydrit-Umwandlung. Dies weist darauf hin, daß - besonders bei synthetischem Gips - verschiedene Gipsarten vorkommen.
Um das geeignete Modell für die Gips/Halbhydrat- bzw. die Halbhydrat/Anhydrat-Umwandlung zu finden, wurden fünfzehn Gleichungen getestet. Keines der Modelle entsprach allen Proben. Die beste Gleichung für die Gips/Halbhydratumwandlung von drei Proben war eine Reaktionsordnungsgleichung, während sich für die Halbhydrat/Anhydratumwandlung von vier Proben als beste Gleichung ein Potenzgesetz ergab. Unterschiede in der Kristallitcharakteristik scheinen eine der Hauptgründe für die unterschiedliche Kinetik der einzelnen Proben zu sein.